



Article

Photoelectrochemical Behavior of the Ternary Heterostructured Systems CdS/WO₃/TiO₂

Anna A. Murashkina¹, Tair V. Bakiev¹, Yurii M. Artemev¹, Aida V. Rudakova¹ ,
Alexei V. Emeline¹ and Detlef W. Bahnemann^{1,2,*} 

¹ Laboratory “Photoactive Nanocomposite Materials”, Saint-Petersburg State University, Ulyanovskaya Str. 1, Peterhof, 198504 Saint-Petersburg, Russia; murashkinaaa@mail.ru (A.A.M.); tairbakievwork@gmail.com (T.V.B.); yuriim54@yandex.ru (Y.M.A.); arudakova@mail.ru (A.V.R.); alexei.emeline@spbu.ru (A.V.E.)

² Institute for Technical Chemistry, Leibniz University of Hannover, Callinstrasse 3, 30167 Hannover, Germany

* Correspondence: bahnmann@iftc.uni-hannover.de

Received: 14 November 2019; Accepted: 22 November 2019; Published: 27 November 2019



Abstract: In this article, we report the results of comparative studies of photoelectrochemical behavior of the binary CdS/TiO₂ and WO₃/TiO₂ and ternary CdS/WO₃/TiO₂ heterostructures based on titania nanotube and planar structures. Physical–chemical characterization by XRD, XPS, and electron microscopy methods together with electrochemical impedance spectroscopy measurements confirm a successful formation of heterostructured electrodes, both nanotube-based and planar. The results of photoelectrochemical studies of the heterostructures demonstrate a significant difference in their behavior depending on the structure geometry and the character of the formed heterojunctions. It is concluded that nanotube-based heterostructure electrodes can be characterized by a stochastic set of different heterojunctions while planar systems demonstrate well-ordered heterojunctions with a strictly defined electron transfer direction. Particularly, we demonstrate the possibility of the realization of Z-scheme of photoexcitation and charge separation in ternary planar systems under visible light irradiation.

Keywords: heterojunctions; heterostructures; Z-scheme; planar structures; nanotubes; titanium dioxide; cadmium sulfide; tungsten trioxide

1. Introduction

During the last decade, a clearly pronounced trend in the field of heterogeneous photocatalysis is the deliberate construction of novel photocatalytic systems based on the semiconductor heterostructures, which are able to absorb solar light and convert its energy into redox chemical reactions [1,2].

By the term “heterostructure”, we mean an integration of two or more semiconductors into an indivisible light absorbing system with interphase boundaries (heterojunctions), and the semiconductor components interacting by means of energy/charge transfer. As expected, the heterostructures can promote (i) an extension of the light absorption spectrum toward longer wavelengths, and consequently, a better utilization of incident solar irradiation; (ii) a minimization of energy losses when the system transforms to a state in which it becomes capable of participating in redox heterogeneous chemistry.

So far, major attention has been given to the creation and investigation of heterostructured photoactive materials of type II [3] composed of two (or more) semiconductors with different band gaps and corresponding positions of the valence and conduction bands as presented in Figure 1a. In general, type II heterostructures are able to absorb light in a wider spectral range; however, the redox ability of such systems (which in a simplified model is determined by the relative positions of the electron and hole energy levels at quasi-stationary states of the system under irradiation) is less than

the redox ability of each individual component of the heterostructure. In other words, the type II heterostructure system is only capable of driving photochemical processes with $|\Delta G|$ smaller than each single semiconductor component of heterostructure in spite of the wide spectral range of photoactive light absorption. As a result, such systems could be inefficient in most desired photochemical redox processes, such as water decomposition or CO_2 reduction to produce “solar fuel” [4].

In 2013, J. Yu and coauthors reported the results of an experimental demonstration of direct Z-scheme performance in photocatalytic process [5]. Since then, a rapid growth of studies directed toward the realization of direct solid-state Z-scheme (see Figure 1b) has been observed [6].

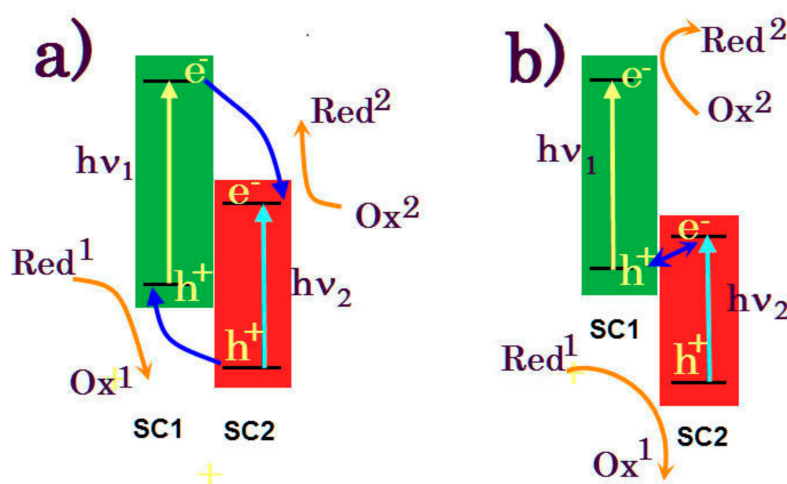


Figure 1. (a) Type II heterojunction, (b) all solid state direct Z-scheme; SC1 and SC2 are semiconductor components of heterostructure.

Should the direct Z-scheme be truly created, the reduction potential of such heterostructure systems under irradiation would correspond to the energy of the bottom of the conduction band of the SC1 component and the oxidation potential of heterostructure would relate to the energy of the top of the valence band of the SC2 component. Therefore, the difference of redox potentials becomes significantly larger than the redox potentials of each component of the heterostructures and therefore, such heterostructures are able to drive photochemical processes with large $|\Delta G|$. At the same time, the spectral range of photoactivity of Z-scheme heterostructures is also extended (similar to type II heterostructures) and light energy absorbed by both components of the heterostructure is used to initiate and to drive redox reactions.

N. Serpone and A.V. Emeline [7] have proposed a three-component nanostructure. According to the proposed scheme, two narrow-band semiconductors absorb light energy and transfer it in electronic form to a wide-band semiconductor, which initiates a consequent redox reaction. In addition, the wide-band gap semiconductor covering the narrow band gap components protects them from corrosion and decomposition in the photochemical side reactions. Therefore, a ternary heterostructure system should demonstrate all the advantages of the direct all-solid Z-scheme in terms of the expanded spectral range of photoexcitation and redox ability together with higher photochemical stability. To create such a ternary heterostructure system, three semiconductors with different band gaps, CdS, WO_3 , and TiO_2 , can be used (see Figure 2).

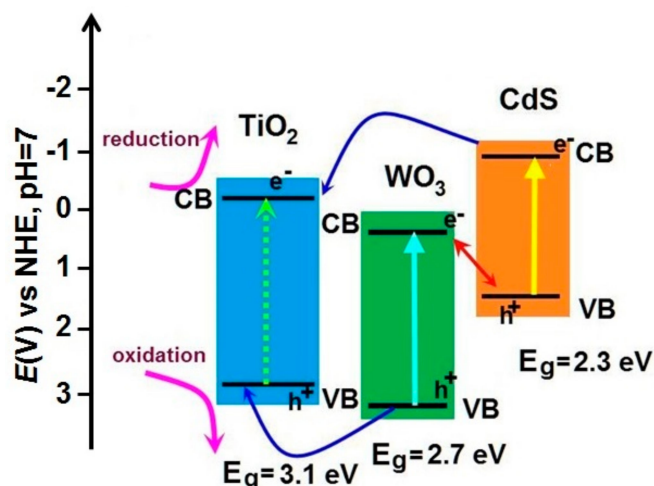


Figure 2. Ternary CdS/WO₃/TiO₂ heterostructure realizing direct all solid Z-scheme.

As emphasized by other authors, photocatalytic tests imply that the construction of multiple component heterostructures favors achieving an efficient separation of photo-generated electrons and holes. For instance, H. Zhang and coauthors recently demonstrated [8] that the Bi₂MoO₆/WO₃/Ag₃PO₄ heterostructure's photocatalytic performance exceeded the photoactivity of its single components, pristine Ag₃PO₄, WO₃/Ag₃PO₄ and Bi₂MoO₆/Ag₃PO₄, by 3.16 times, 2.63 times, and 1.75 times, respectively.

The two-component TiO₂/CdS heterostructure has been under investigation for a long time [9], first as a sensitized TiO₂ system. This system continuously attracts attention due to relative simplicity of its formation and promising potential for solar fuel production, together with other valuable products [10,11]. Nowadays, some researchers report that the direct Z-scheme heterojunction can be easily realized in this system. For instance, J. Low et al. have provided strong evidence based on ISI-XPS characterization, hydroxyl radical generation test, and DFT simulation, that confirms the formation of the direct Z-scheme heterojunction between TiO₂ and CdS [12].

The TiO₂/WO₃ heterostructured system, used as photocatalyst, has been also highlighted in numerous publications [13]. The reported results of photocatalytic behavior of such a heterostructure are very promising. S. Prabhu et al. [14] claim that the TiO₂/WO₃ heterostructures show 17 times higher photon-to-hydrogen conversion efficiency than pure TiO₂ and WO₃ under solar light and almost complete removal of organic pollutants in 60 min under visible light.

TiO₂/CdS/WO₃ ternary heterostructure was also recently studied [15]. CdS and WO₃ were used in the form of hierarchical WO₃-nanosheet/CdS-nanorod arrays to produce a heterostructure, and TiO₂ was used as a protection layer. This type II heterojunction photoanode demonstrated a photocurrent density of 5.4 mA cm⁻² at 0.8 V versus a reversible hydrogen electrode for sulfite oxidation that is 12 times greater than that of WO₃-nanosheet array (0.45 mA cm⁻²) and 3 times higher than CdS-nanorod arrays (1.85 mA cm⁻²). The authors suppose that the favorable heterojunction between WO₃ and CdS enhances the charge separation efficiency and widens the light absorption spectrum.

In this study, we performed a comparative exploration of photoelectrochemical behavior of the binary CdS/TiO₂ and WO₃/TiO₂ and ternary CdS/WO₃/TiO₂ heterostructures based on titania nanotube and planar structures. Particularly, we demonstrated the possibility for the realization of Z-scheme of photoexcitation and charge separation in planar heterostructured systems.

2. Results

Figure 3 demonstrates linear sweep voltammetry (LSV) dependencies obtained for both nanotube (Figure 3a) and planar (Figure 3b) electrodes under irradiation. Corresponding dependencies recorded under dark conditions are given in Figure S1 (Supplementary Materials).

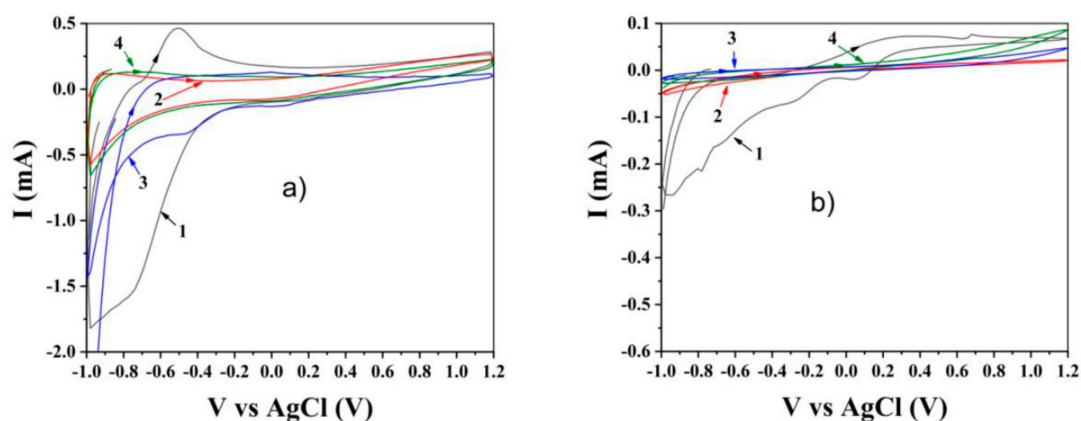


Figure 3. Linear sweep voltammetry (LSV) curves. Potential scan rate: 20 mV/s. Irradiation—1 Sun. (a) nanotube-based electrodes: 1—TiO₂, 2—CdS/TiO₂, 3—WO₃/TiO₂, 4—WO₃/CdS/TiO₂; (b) planar electrodes: 1—TiO₂, 2—CdS/TiO₂, 3—WO₃/TiO₂, 4—CdS/WO₃/TiO₂.

As evident from the presented data, both nanotube-based and planar TiO₂ electrodes demonstrate a significant hysteresis typical for TiO₂ both in the dark and under irradiation, originating from the charging-discharging intrinsic defect states at the surface and in the near-surface spatial region of TiO₂. However, the hysteresis is significantly changed and diminished in the case of formation of binary and ternary heterostructures. This indicates, on the one hand, a successful formation of heterojunctions between semiconductors and on the other hand, an appearance of new charge transfer pathways that play a dominant role in the heterostructures. In other words, formation of heterostructures significantly screens the effects of defect states becoming a major factor in photoelectrochemical processes. For further discussion, it is wise to note the similarity of the curves obtained for binary CdS/TiO₂ and ternary CdS/WO₃/TiO₂ nanotube-based heterostructures, which suggests that CdS plays a significant role in both heterostructures.

Formation of binary and ternary heterostructures is also confirmed by the results of electrochemical impedance spectroscopy (EIS). It is commonly known that EIS analysis provides information about the interfacial properties of electrodes [16]. Figure 4 demonstrates the EIS dependencies obtained for both nanotube (Figure 4a) and planar (Figure 4b) electrodes under irradiation. Corresponding dependencies measured in the dark are presented in Figure S2 (Supplementary Materials).

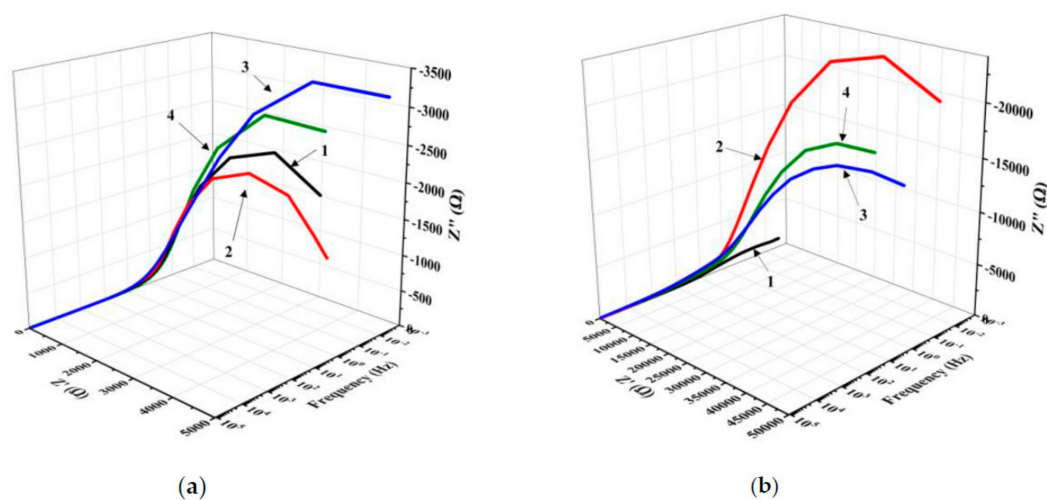


Figure 4. 3D EIS plots recorded under irradiation. (a) nanotube-based electrodes: 1—TiO₂, 2—CdS/TiO₂, 3—WO₃/TiO₂, 4—WO₃/CdS/TiO₂; (b) planar electrodes: 1—TiO₂, 2—CdS/TiO₂, 3—WO₃/TiO₂, 4—CdS/WO₃/TiO₂.

These dependencies can be presented in the form of the EIS Nyquist plots (see Figures S3 and S4 in Supplementary Materials). The curvature of the semicircle in EIS Nyquist plot is related to the electron transfer resistance, which reveals electron transfer kinetics of the redox pair at the electrode/electrolyte interface. As indicated in the Section 5, the character of behavior of the electrodes in the dark and under the irradiation can be simulated by the equivalent circuit scheme presented in Figure 5.

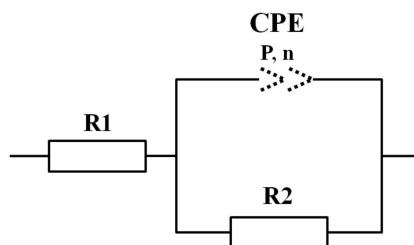


Figure 5. Equivalent circuit scheme used for mathematical treatment of the experimental impedance dependencies.

Calculated values of the active resistances and parameters of CPE are given in Table 1 for nanotube-based systems and in Table 2 for planar heterostructures, respectively (corresponding parameters measured in the dark are given in the Tables S1 and S2).

Table 1. Parameters of equivalent circuit scheme for nanotube-based systems under irradiation.

Sample	R1	R2	P	n
TiO ₂	~0	3000 ± 1000	0.0005 ± 0.00004	0.7 ± 0.2
CdS/TiO ₂	~0	3000 ± 1000	0.0005 ± 0.00003	0.7 ± 0.1
WO ₃ /TiO ₂	~0	9000 ± 4000	0.0005 ± 0.00002	0.6 ± 0.1
CdS/WO ₃ /TiO ₂	~0	2000 ± 2000	0.0005 ± 0.00007	0.7 ± 0.2

Table 2. Parameters of equivalent circuit scheme for planar systems under irradiation.

Sample	R1	R2	P	n
TiO ₂	~0	9300 ± 400	0.000308 ± 0.000009	0.55 ± 0.01
CdS/TiO ₂	300 ± 200	63,000 ± 1000	0.000062 ± 0.000001	0.82 ± 0.01
WO ₃ /TiO ₂	400 ± 200	56,000 ± 2000	0.000044 ± 0.000002	0.58 ± 0.02
CdS/WO ₃ /TiO ₂	300 ± 200	50,000 ± 2000	0.000008 ± 0.000003	0.69 ± 0.02

A comparative analysis of the equivalent circuit scheme parameters, measured in the dark and under irradiation, shows that in the dark, the impedances of CPE in both nanotube-based and planar heterosystems demonstrate a capacitor behavior ($n \rightarrow 1$) with essentially large resistance R2 as is typical for heterostructures due to barrier formation at the heterojunctions. However, under irradiation, the impact of the capacitor behavior is significantly reduced ($n \ll 1$) as well as both active and reactive resistances also decrease (R2 and P). This indicates that photoexcitation of the heterosystems results in the generation of free charge carriers in all semiconductor components of the heterostructures, which in turn, decreases the barriers in the corresponding heterojunctions. Thus, photoexcitation opens pathways for effective electron transfer through the heterostructures.

From the presented data, one can conclude that in the set of nanotube electrodes, the resistance increases as $\text{WO}_3/\text{TiO}_2 \gg \text{TiO}_2 \approx \text{CdS}/\text{TiO}_2 \geq \text{CdS}/\text{WO}_3/\text{TiO}_2$ while other characteristics remain nearly the same. It implies that WO_3 in contact with Ti support creates an extra Ohmic resistance while for all other nanotube systems, a major contribution to resistance belongs to the titania nanotubes. At the same time, for the planar electrodes, the resistance changes as $\text{CdS}/\text{TiO}_2 \geq \text{WO}_3/\text{TiO}_2 \geq \text{CdS}/\text{WO}_3/\text{TiO}_2 \gg \text{TiO}_2$ since the formation of planar heterojunctions

increases the resistance of the electrodes. However, the ternary system demonstrates the minimal resistance comparing to binary systems.

Another presentation of the EIS dependencies can be done in the form of Bode plots as shown in Figure 6 and Figure S5. Figure 6 shows EIS Bode plots for both nanotube (Figure 6a) and planar (Figure 6b) electrodes under irradiation. Corresponding dependencies plotted under the dark conditions are presented in Figure S5 (Supplementary Materials).

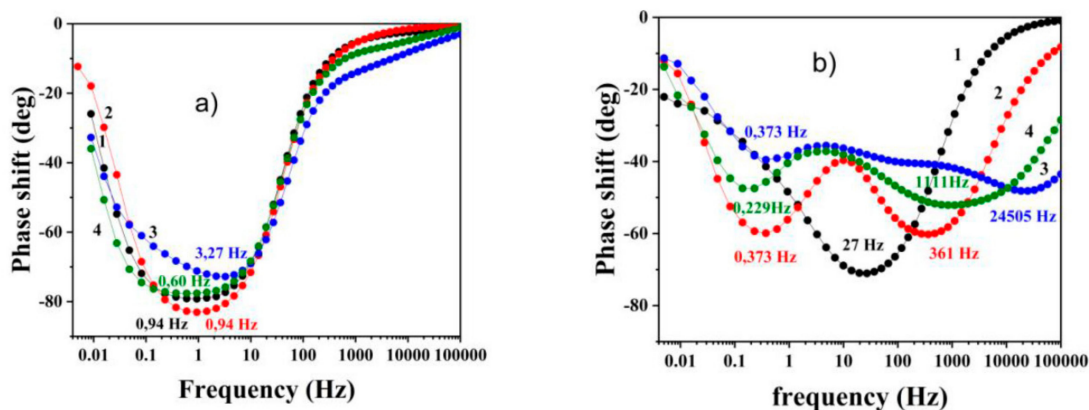


Figure 6. EIS Bode plots obtained under irradiation. (a) nanotube-based electrodes: 1—TiO₂, 2—CdS/TiO₂, 3—WO₃/TiO₂, 4—WO₃/CdS/TiO₂; (b) planar electrodes: 1—TiO₂, 2—CdS/TiO₂, 3—WO₃/TiO₂, 4—CdS/WO₃/TiO₂.

Bode plots show a clear difference between nanotube and planar systems. It is evident that the planar systems' behavior describes (at least) two different processes reflected by the presence of two phase shift extrema while nanotube systems demonstrate clearly only a single extremum. This difference can be assumed to be due to the difference in geometric structure between two types of heterostructures. Indeed, a large part of nanotube-based heterostructures consists of titania nanotubes and heterojunctions play a minor role in the system, while in planar heterosystems, a key-role in the photoelectrochemical behavior belongs to the heterojunctions between semiconductors. At the frequency where a maximum $Z''(\omega)$ is observed, the straightforward relationship $1/\omega_{\max} = 1/(2\pi f_{\max}) = \tau$, where τ is a time constant of the electrochemical reaction, indicates the time scale of an electrochemical reaction [17]. Accordingly, a certain time constant can be ascribed to each extremum (see Tables 3 and 4 for nanotube-based and planar heterostructures under irradiation, respectively).

Table 3. The time constants τ calculated from Bode diagrams for nanotube heterostructures under irradiation.

Sample	Frequency, Hz	τ , s
TiO ₂	0.94	0.169
CdS/TiO ₂	0.94	0.169
WO ₃ /TiO ₂	3.27	0.0487
CdS/WO ₃ /TiO ₂	0.6	0.265

Table 4. The time constants τ calculated from Bode diagrams for planar heterostructures under irradiation.

Sample	Frequency, Hz	τ , s
TiO ₂	27	0.006
CdS/TiO ₂	0.373	0.427
CdS/TiO ₂	361	0.0004
WO ₃ /TiO ₂	0.373	0.427
WO ₃ /TiO ₂	24,505	6.49×10^{-6}
CdS/WO ₃ /TiO ₂	0.229	0.695
CdS/WO ₃ /TiO ₂	1111	0.000143

Comparing the values τ obtained for nanotube-based and planar heterostructures, one may conclude that this characteristic time parameter is much shorter for planar systems compared to nanotube based ones. This difference can be attributed to geometry (thickness) of the corresponding electrodes since nanotube-based structures are much thicker. Photoexcitation of the heterostructure electrodes results in significant decay of τ , regardless of the geometry of the electrodes.

It is also wise to note that the maximal values of τ are observed for the ternary heterostructure systems, both nanotube-based and planar, since the complex character of heterojunctions in such systems makes a pathway for charge carriers significantly “longer” compared to simpler structures.

Figure 7 demonstrates the transient kinetics of photocurrent behavior for both nanotube and planar electrodes when light irradiation is switched on.

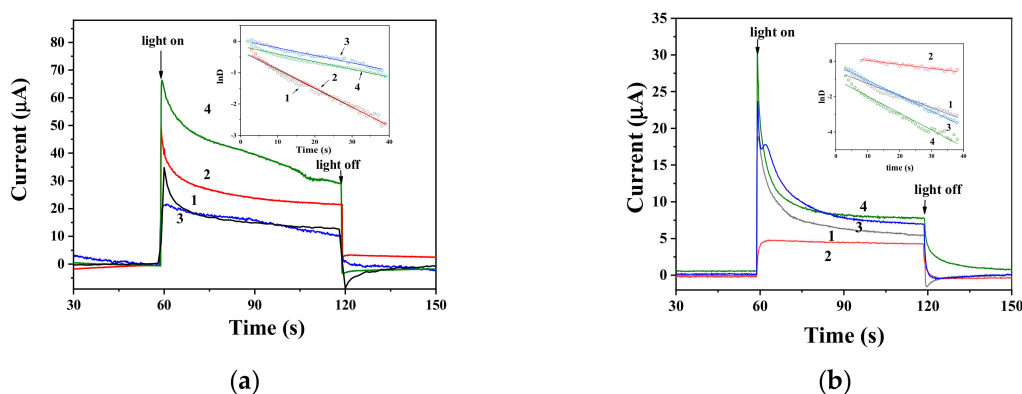


Figure 7. Transient photo-current responses of electrodes: (a) nanotube-based electrodes: 1—TiO₂, 2—CdS/TiO₂, 3—WO₃/TiO₂, 4—WO₃/CdS/TiO₂; (b) planar electrodes: 1—TiO₂, 2—CdS/TiO₂, 3—WO₃/TiO₂, 4—CdS/WO₃/TiO₂. Insertions show the semi-logarithmic representations of the corresponding photo-current response dependencies.

The transient photocurrent decay is observed immediately after the illumination start (see Figure 7), approaching to the stationary photocurrent for both nanotube and planar heterostructured electrodes. It is assumed that the photocurrent decays due to an enhancement of photogenerated electron-hole recombination and approaches a quasi-steady state value when the rates of electron-hole photogeneration and recombination become equal. Note, that the samples of ternary composition (both planar and nanotubes) show the highest initial photocurrent values and the slowest approach to the steady state. The transient time constant (τ_{dec}) calculated by Equation (1), can be a characteristic of the efficiency of the system transition to quasi steady state behavior:

$$\ln D = -\frac{t}{\tau_{dec}}, \quad (1)$$

where D is the transient photocurrent decay:

$$D = \frac{I_t - I_s}{I_i - I_s} \quad (2)$$

where I_t is the photocurrent generated at time t , I_s is the steady state photocurrent, and I_i is the initial photocurrent.

Calculated values of τ_{dec} for both nanotube-based and planar systems are presented in Table 5.

Table 5. Transient time constants, τ_{dec} .

Planar		Nanotube-Based	
Sample	τ_{dec} s	Sample	τ_{dec} s
TiO ₂	1.8 ± 0.2	TiO ₂	16.8 ± 0.6
CdS/TiO ₂	45 ± 2	CdS/TiO ₂	16.4 ± 0.2
WO ₃ /TiO ₂	4.8 ± 0.6	WO ₃ /TiO ₂	41 ± 2
CdS/WO ₃ /TiO ₂	0.98 ± 0.07	CdS/WO ₃ /TiO ₂	42 ± 2

One can note that in the case of nanotube-based structures, the values τ_{dec} for CdS/TiO₂ and TiO₂ systems are about the same. Similar values τ_{dec} are also obtained for WO₃/TiO₂ and CdS/WO₃/TiO₂ systems. Therefore, the difference in τ_{dec} for these two groups can be attributed to the contact with higher resistance between WO₃ and Ti substrate, and in the absence of WO₃, the contact with the substrate is formed by TiO₂ nanotubes only. Again, these results confirm the conclusions made from EIS data analysis that the major role in all nanotube-based systems is played by the titania nanotubes, while the heterojunctions have a minor effect on electronic processes in such electrodes. At the same time, the τ_{dec} values determined for planar samples are significantly different, which is most likely dictated by the difference in semiconductor heterojunctions formed in different planar heterostructures.

Spectral dependencies of incident photon-to-current conversion efficiency, IPCE, measured for both nanotube-based and planar heterostructures, are shown in Figure 8.

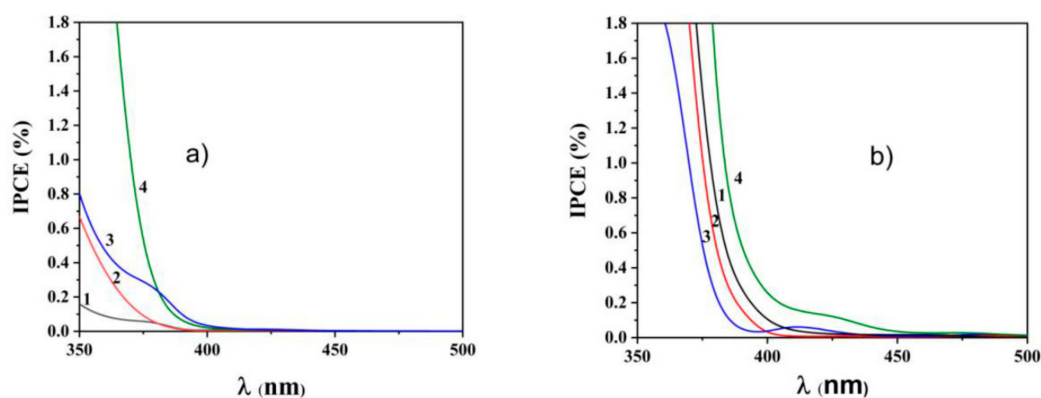


Figure 8. Spectral dependencies of the incident photon-to-current conversion efficiency (IPCE) in the near UV and visible range: (a) nanotube-based electrodes: 1—TiO₂, 2—CdS/TiO₂, 3—WO₃/TiO₂, 4—WO₃/CdS/TiO₂; (b) planar electrodes: 1—TiO₂, 2—CdS/TiO₂, 3—WO₃/TiO₂, 4—CdS/WO₃/TiO₂.

As evident from the presented spectral dependencies in the spectral region of fundamental absorption of TiO₂ (and therefore, of all components of the heterostructures), the highest IPCE is observed for ternary heterostructures regardless of their geometry (planar vs. nanotube). At the same time, there is a significant difference in the way the binary heterosystems affect the IPCE in the UV-spectral region depending on whether they are planar or nanotube based: For nanotube systems, the IPCE for binary systems (both WO₃/TiO₂ and CdS/TiO₂) is higher than for TiO₂ nanotubes, while for

planar heterosystems, the IPCE registered for binary systems are lower than for pristine TiO_2 electrode in accordance with the increase of resistance.

A remarkable difference for ternary heterosystems with respect to their geometry is observed in the visible spectral range: No significant photoactivity is detected for nanotube based heterosystems, while an essential photoresponse is observed for planar heterostructure electrode within the spectral range of 400–450 nm. Therefore, planar ternary heterostructure systems demonstrate strong photoactivity in the visible spectral range compared to both pristine TiO_2 and binary heterostructure electrodes. It is wise to emphasize that the spectral edge of photoactivity at 450 nm corresponds well to the band gap of WO_3 (~2.75 eV). In other words, the ternary planar heterostructured system shows its activity when both narrow band gap semiconductors, WO_3 and CdS, are photoexcited in the fundamental absorption spectral region. This behavior of IPCE spectral dependence confirms our conclusion inferred from LSV data, that formation of heterojunctions is a major factor which determines the efficiency of photoelectrochemical process and significantly reduces the possible role of defect states in semiconductors. Taking into consideration the geometry of the planar ternary system, one may conclude that its photoactivity under visible light irradiation is possible only in the case when Z-scheme scenario of photoexcitation and charge separation is realized.

3. Discussion

Before starting an analysis of experimental results yielding the possible mechanisms of electrochemical behavior of heterostructured systems, it is wise to recall the geometry of the formed electrodes. Figure 9 represents an expected geometry of the formed ternary heterostructures.

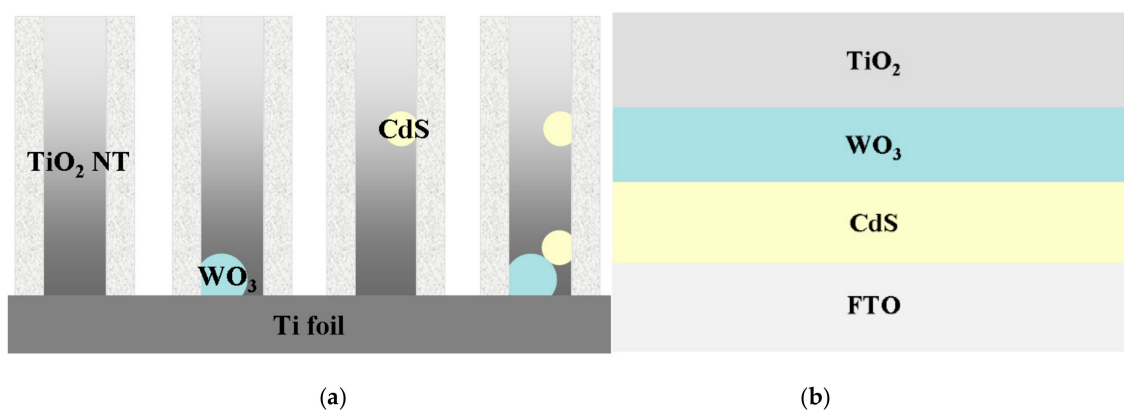


Figure 9. Geometry structures of the heterostructured electrodes: (a) nanotube-based; (b) planar.

As seen in Figure 9, the nanotube-based heterostructure electrode is characterized by a rather random distribution of narrow band gap semiconductor components in titania nanotubes due to the methods applied for their synthesis and formation. Based on the data provided by electron microscopy, one may expect that a significant part of titania nanotubes remains undecorated with narrow band gap semiconductors. At the same time, statistically, some nanotubes can be modified with only one of the components of the ternary system, either with WO_3 or with CdS. Obviously, a probability that titania nanotubes form heterostructures with both WO_3 and CdS and heterojunction between these narrow band gap semiconductors is not high. Therefore, ternary nanotube-based heterostructure electrodes consist of unmodified titania nanotubes and stochastically random sets of different heterojunctions, such as WO_3/TiO_2 and CdS/TiO_2 only, a combination of both WO_3/TiO_2 and CdS/TiO_2 , and $\text{CdS}/\text{WO}_3/\text{TiO}_2$ in different nanotubes. Accordingly, it creates a possibility for various electron transfer processes within nanotube-based electrodes as demonstrated in Figure 10a.

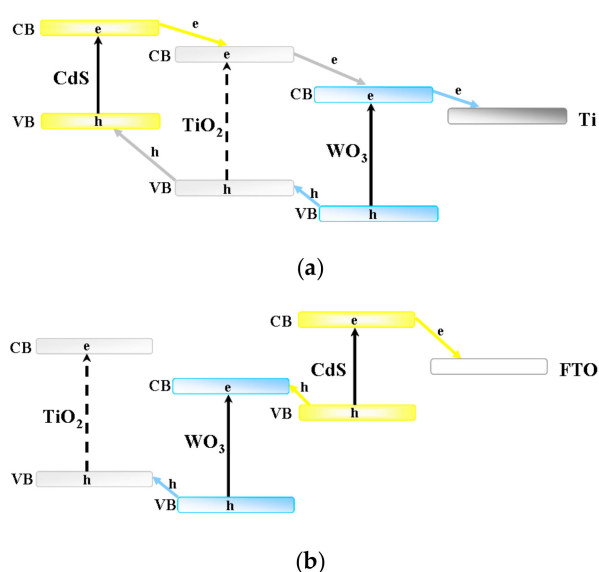


Figure 10. An energy structure and directions of electron transfer in ternary heterostructured systems: (a) nanotube-based; (b) planar.

On the other hand, one may expect a completely different scenario for the ternary planar system, whose geometric layer-by-layer structure is well ordered due to the approach applied for its formation. Accordingly, there is only a limited and specific set of electron transfer processes that may occur in such heterostructure electrodes, as demonstrated in Figure 10b. Accordingly, photoexcitation in the visible spectral range can lead to electrochemical activity of the ternary planar system only if both WO₃ and CdS components are photoexcited. Otherwise, the heterojunction barriers would prevent charge carrier migration from the outer surface of TiO₂ layer to the contact layer at the FTO substrate. By contrast, in nanotube-based systems, the outer surface of TiO₂ is in direct contact with the Ti substrate through titania nanotubes. Therefore, the heterojunctions formed with narrow band gap semiconductors play a rather minor role in charge carrier migration. Summing up, we conclude that ternary planar systems demonstrate their photoactivity due to realization of Z-scheme of photoexcitation and charge separation.

4. Materials and Methods

4.1. Preparation of TiO₂ Nanotubes and Binary (CdS/TiO₂, WO₃/TiO₂) and Ternary (CdS/WO₃/TiO₂) Heterostructure Systems

TiO₂ nanotubes (TNT) were prepared by anodic oxidation of Ti-foil (99.99%) in ethylene glycol electrolyte containing ammonium fluoride (0.1 wt %) with deionized water (2 vol %). All anodization processes were performed in a conventional two-electrode electrochemical cell with titanium foil as an anode and platinum foil as a cathode at constant voltage (60.0 V) at room temperature for 2.5 h. After anodization was completed, the samples were washed with deionized water and dried at 100 °C followed by annealing at 500 °C for 2 h (heating/cooling rate of 30 °C/h) to transform amorphous TiO₂ to crystalline phase.

The binary WO₃/TiO₂ heterostructure system was formed by electrochemical deposition of tungsten on the Ti foil by using sodium tungstate (1M) as a W precursor and a mixture of dimethylformamide and formamide (volume ratio 1/9) as an electrolyte. The electrochemical deposition was carried out for 1 h at potential −2.0 V. Thereafter, the substrate was washed with deionized water. Then, the obtained substrate was used as an anode for anodization process to form TiO₂ nanotubes at the same conditions as reported above.

The electrochemical deposition of CdS was performed using the obtained TiO₂ and WO₃/TiO₂ samples as working electrodes in an aqueous electrolyte containing 0.002 M CdSO₄ and 0.1 M Na₂S₂O₄

at pH = 7. An electrochemical reduction of bisulfate ions to sulfide ions followed by deposition in the form of CdS at TiO₂ nanotubes surface, was performed at the potential −0.6 V for 30 min.

4.2. Preparation of TiO₂ Films, and Binary (CdS/TiO₂, WO₃/TiO₂) and Ternary (CdS/WO₃/TiO₂) Planar Heterostructure Systems

All planar systems were deposited on FTO glass substrates, preliminarily washed in acetone for 30 min using ultrasound bath and dried at 200 °C.

The TiO₂ polycrystal dense layer in all planar systems was formed by a sol-gel dip coating method (KSV Nima dip-coater). TiO₂ sol was produced using 9 mL titanium isopropoxide, 100 mL isopropyl alcohol, and 18 g citric acid, which were thoroughly mixed and left to age for 24 h. The dense TiO₂ film was formed by immersion into sol solution four consecutive times with withdrawing velocity of 10 mm min^{−1} and drying the deposited film for 30 min before next immersion. Then, films were annealed at 450 °C in air for 5 h to crystallize the film and to remove all residual organics.

CdS polycrystal layer was chemically formed on FTO glass support for both binary and ternary CdS-containing heterostructured systems by deposition from the aqueous solution prepared by mixing 0.1 M ammonia as a stabilizer, 0.002 M thiourea as a reducing agent, and 0.001 M CdSO₄ as a precursor. The deposition was carried out in thermostatic conditions at 70 °C for 30 min. After film deposition, the electrodes were washed with deionized water and dried at 100 °C.

WO₃ polycrystal layers were formed on either FTO glass or CdS/FTO substrates by the dip coating method. A WO₃ sol solution was prepared from WO₃ powder (2 wt %) dissolved in concentrated ammonia at 60 °C. An immersion was carried out consequently eight times with withdrawing velocity of 10 mm min^{−1} and drying at 200 °C for 15 min after each immersion. Then, samples were annealed at 450 °C at the air for 5 h.

As a result, the following layered samples, TiO₂, WO₃/TiO₂, CdS/TiO₂, CdS/WO₃/TiO₂, were formed on FTO glass substrates and the TiO₂ layer was always on top of the planar heterostructured electrodes.

4.3. Material Characterization

X-ray diffraction method was used to analyze phase formation with Bruker “D8 DISCOVER” high-resolution diffractometer (CuK_α radiation) in the angle range of 20° ≤ 2θ ≤ 80° at a scanning speed 5.0°/min. The data analysis by the Rietveld method was carried out using the TOPAS (Bruker AXS) software. According to XRD analysis, the produced samples, both nanotubes and planar, were crystallized in the phases corresponding to the desired components of heterostructures (TiO₂ anatase, CdS, WO₃ (monoclinic)) (see Figure S6 in the Supplementary Materials).

The surface morphology was explored by scanning electron microscopy (Zeiss Supra 40 VP system) for all synthesized semiconductor electrodes (see Figures S7 and S8). As evident from SEM images, the titanium dioxide nanotube layer was uniformly distributed on the substrate, the pores in the obtained layer were normally oriented to the substrate plate. The diameter of the tubes was about 70 nm and its thickness (nanotube length), about 1 μm. Electron microscopy images of planar systems confirm a successful deposition of the layers of each component of the heterostructures (see Figure S8) and formation of the dense outer layer of TiO₂ reliably covering and protecting inner layers of the heterostructures.

To validate the presence of narrow band gap semiconductors in the titanium dioxide nanotubes, the XPS spectra of the heterostructure systems were examined. The spectra are presented in Figure S9 (see Supplementary Materials). The peaks related to the binding energies ~458.4 eV and ~464.2 eV, correspond to Ti2p_{3/2} and Ti2p_{1/2}, respectively. According to the reference data [18], Ti⁴⁺ is the dominant oxidation state of titanium ions in nanotubes. The peaks at binding energies of 35.5 eV, 405.1 eV, and 168.5 eV in the XPS spectra of the ternary heterostructure system correspond to the W4f, Cd3d, and S2p states, respectively. The O1s peak at ~529.60 eV demonstrates a symmetric shape for

both pristine titania nanotubes and ternary system. Thus, the O1s XPS spectra give no evidence of the presence of more than one type of oxygen state.

4.4. Photoelectrochemical Experiments

Photoelectrochemical measurements were performed at room temperature in a three-electrode cell with a quartz window. All potential measurements were performed against the Ag/AgCl reference electrode (0.222 V vs. potential of NHE). Platinum wire was used as a counter electrode. Na₂SO₄ (1M) aqueous solution was used as an electrolyte. A computer-controlled ZAHNER CIMPS-2 (ZAHNER-elektrik, GmbH & Co. KG, Germany) potentiostat was used for electrochemical measurements. The dependences of photocurrent on intensity and wavelength of acting light were carried out with the setup of CIMPS-LED light sources.

The incident photon-to-current conversion efficiency (IPCE) values were calculated using the following equation [19]:

$$IPCE(\%) = \frac{1239.8 \cdot j_{ph}}{I_{mchr} \cdot \lambda} \times 100\%, \quad (3)$$

where 1239.8 (in V·nm) is a multiplication of Planck's constant, h , and the speed of light, c ; j_{ph} (in mA·cm⁻²) is the photocurrent density that was taken from chronoamperometry measurements; I_{mchr} (in mW·cm⁻²) is the power density of acting monochromatic light; and λ (in nm) is the wavelength of this monochromatic light.

To treat the impedance dependences and to obtain the heterostructure characteristics, the following equivalent circuit scheme was applied (see Figure 5). The scheme containing constant phase element (CPE) was chosen as physically more realistic and providing a better approximation to experimental dependencies. An impedance of CPE is given by Equation (4):

$$Z_{CPE} = \frac{1}{P\omega^n} e^{-\frac{\pi}{2}ni}, \quad (4)$$

where P and n ($0 < n < 1$) are frequency independent parameters. Note that the case $n = 1$ describes an ideal capacitor, while the case $n = 0$ describes a pure resistor [20].

Graphical treatment of impedance measurements was performed applying two approaches: Nyquist plot and Bode plot.

5. Conclusions

Summing up, we may conclude that the types of semiconductors forming heterojunctions and their band energy structures are not the only factors that determine the photoelectrochemical behavior of ternary heterostructures. A significant role is also given to geometry of heterostructures (that is an order of components in heterostructure, see Figure 9), which dictates the major direction of charge transfer in ternary systems under photoexcitation. This is clearly demonstrated for ternary planar systems when their photoactivity under visible light is possible only due to realization of Z-scheme of photoexcitation and charge separation (that provides a condition for electron migration from the outer TiO₂ surface through the whole heterostructure to FTO substrate).

Supplementary Materials: The following are available online at <http://www.mdpi.com/2073-4344/9/12/999/s1>, Figure S1: Linear sweep voltammetry (LSV) curves recorded under the dark conditions, Figure S2: 3D EIS plots recorded in the dark, Figure S3: EIS Nyquist plots recorded in the dark, Figure S4: EIS Nyquist plots. Data recorded under illumination, Figure S5: EIS Bode plots. Data recorded under dark conditions, Figure S6: XRD patterns of planar samples and nanotubes, Figure S7: SEM images of the titania nanotube (TNT) based systems, Figure S8: SEM images of planar systems on FTO glass substrates, Figure S9: XPS spectra, Table S1: Parameters of equivalent circuit scheme for nanotube-based systems in the dark, Table S2: Parameters of equivalent circuit scheme for planar systems in the dark, Table S3: The time constants τ calculated from Bode diagrams for nanotube heterostructures in the dark, Table S4: The time constants τ calculated from Bode diagrams for planar heterostructures in the dark.

Author Contributions: Conceptualization, A.V.E.; methodology, A.V.E. and A.A.M.; validation, T.V.B., A.V.R., and Y.M.A.; formal analysis, T.V.B. and A.A.M.; investigation, A.A.M., T.V.B.; writing—Original draft preparation, A.V.E., Y.M.A., A.V.R. and T.V.B.; writing—Review and editing, A.V.E. and D.W.B.; visualization, A.V.R., T.V.B., and Y.M.A.; supervision, A.V.E. and D.W.B.

Funding: This research was funded by Russian Foundation for Basic Research (RFBR) via a research Grant 18–29–23035 mk and the Saint-Petersburg State University via a Research Grant (Pure ID 32706707).

Acknowledgments: We are grateful to the Resource Center (RC) “Nanophotonics”, RC “Nanotechnology”, RC “Chemical Analysis and Materials Research Centre”, RC “X-ray Diffraction Studies” of the Research Park at the Saint-Petersburg State University for helpful assistance in the characterization of the samples.

Conflicts of Interest: The authors declare no conflict of interest.

References

1. Meng, S.; Zhang, J.; Chen, S.H.; Zhang, S.; Huang, W. Perspective on construction of heterojunction photocatalysts and the complete utilization of photogenerated charge carriers. *Appl. Sur. Sci.* **2019**, *476*, 982–992. [[CrossRef](#)]
2. Lianos, P. Review of recent trends in photoelectrocatalytic conversion of solar energy to electricity and hydrogen. *Appl. Catal. Environ.* **2017**, *210*, 235–254. [[CrossRef](#)]
3. He, X.; Zhang, C. Recent advances in structure design for enhancing photocatalysis. *J. Mater. Sci.* **2019**, *54*, 8831–8851. [[CrossRef](#)]
4. Serpone, N.; Emeline, A.V.; Ryabchuk, V.K.; Kuznetsov, V.N.; Artem'ev, Y.M.; Horikoshi, S. Why do Hydrogen and Oxygen Yields from Semiconductor-Based Photocatalyzed Water Splitting Remain Disappointingly Low? Intrinsic and Extrinsic Factors Impacting Surface Redox Reactions. *ACS Energy Lett.* **2016**, *1*, 931–948. [[CrossRef](#)]
5. Yu, J.; Wang, S.; Low, J.; Xiao, W. Enhanced photocatalytic performance of direct Z-scheme g-C₃N₄-TiO₂ photocatalysts for the decomposition of formaldehyde in air. *Phys. Chem. Chem. Phys.* **2013**, *15*, 16883–16890. [[CrossRef](#)] [[PubMed](#)]
6. Low, J.; Jiang, C.; Cheng, B.; Wageh, S.; Al-Ghamdi, A.A.; Yu, J. A Review of Direct Z-Scheme Photocatalysts. *Small Methods* **2017**, *1*, 1700080. [[CrossRef](#)]
7. Serpone, N.; Emeline, A.V. Semiconductor Photocatalysis—Past, Present, and Future Outlook. *J. Phys. Chem. Lett.* **2012**, *3*, 673–677. [[CrossRef](#)] [[PubMed](#)]
8. Zhang, H.; Yu, D.; Wang, W.; Gao, P.; Bu, K.; Zhang, L.; Zhong, S.; Liu, B. Multiple heterojunction system of Bi₂MoO₆/WO₃/Ag₃PO₄ with enhanced visible-light photocatalytic performance towards dye degradation. *Adv. Powder Technol.* **2019**, *30*, 1910–1919. [[CrossRef](#)]
9. Serpone, N.; Pelizzetti, E. (Eds.) *Photocatalysis: Fundamentals and Applications*; Wiley: New York, NY, USA, 1989.
10. Sfaelou, S.; Sygellou, L.; Dracopoulos, V.; Travlos, A.; Lianos, P. Effect of the Nature of Cadmium Salts on the Effectiveness of CdS SILAR Deposition and Its Consequences on the Performance of Sensitized Solar Cells. *J. Phys. Chem. C* **2014**, *118*, 22873–22880. [[CrossRef](#)]
11. Papagiannis, I.; Doukas, E.; Kalarakis, A.; Avgouropoulos, G.; Lianos, P. Photoelectrocatalytic H₂ and H₂O₂ Production Using Visible-Light-Absorbing Photoanodes. *Catalysts* **2019**, *9*, 243. [[CrossRef](#)]
12. Low, J.; Dai, B.; Tong, T.; Jiang, C.; Yu, J. In Situ Irradiated X-Ray Photoelectron Spectroscopy Investigation on a Direct Z-Scheme TiO₂/CdS Composite Film Photocatalyst. *Adv. Mater.* **2019**, *31*, 1802981. [[CrossRef](#)]
13. Sotelo-Vazquez, C.; Quesada-Cabrera, R.; Ling, M.; Scanlon, D.O.; Kafizas, A.; Thakur, P.K.; Lee, T.-L.; Taylor, A.; Watson, G.W.; Palgrave, R.G.; et al. Evidence and Effect of Photogenerated Charge Transfer for Enhanced Photocatalysis in WO₃/TiO₂ Heterojunction Films: A Computational and Experimental Study. *Adv. Funct. Mater.* **2017**, *27*, 1605413. [[CrossRef](#)]
14. Prabhu, S.; Cindrella, L.; Kwon, O.J.; Mohanraju, K. Photoelectrochemical and photocatalytic activity of TiO₂-WO₃ heterostructures boosted by mutual interaction. *Mater. Sci. Semicond. Process.* **2018**, *88*, 10–19. [[CrossRef](#)]
15. Wang, Z.; Yang, G.; Tan, C.h.K.; Nguyen, T.D.; Iing, A.; Tok, Y. Amorphous TiO₂ coated hierarchical WO₃-nanosheet/CdS-nanorod arrays for improved photoelectrochemical performance. *Appl. Surf. Sci.* **2019**, *490*, 411–419. [[CrossRef](#)]

16. Barsoukov, E.; Macdonald, J.R. (Eds.) *Impedance Spectroscopy Theory, Experiment, and Applications*; John Wiley & Sons, Inc.: Hoboken, NJ, USA, 2005.
17. Park, S.-M.; Yoo, J.-S. Electrochemical impedance spectroscopy for better electrochemical measurements. *Anal. Chem.* **2003**, *75*, 455A–461A. [[CrossRef](#)]
18. Crist, B.V. *Handbooks of Monochromatic XPS Spectra; Volume 2—Commercially Pure Binary Oxides*; XPS International LLC: Mountain View, CA, USA, 2005.
19. Chen, Z.; Jaramillo, T.; Deutsch, T.; Kleiman-Shwarsstein, A.; Forman, A.; Gaillard, N.; Dinh, H. Accelerating materials development for photoelectrochemical hydrogen production: Standards for methods, definitions, and reporting protocols. *J. Mater. Res.* **2010**, *25*, 3–16. [[CrossRef](#)]
20. Kochowski, S.; Nitsch, K. Description of the frequency behaviour of metal-SiO₂-GaAs structure characteristics by electrical equivalent circuit with constant phase element. *Thin Solid Films* **2002**, *415*, 133–137. [[CrossRef](#)]



© 2019 by the authors. Licensee MDPI, Basel, Switzerland. This article is an open access article distributed under the terms and conditions of the Creative Commons Attribution (CC BY) license (<http://creativecommons.org/licenses/by/4.0/>).